Rhodium dihydride (RhH$_2$) with high volumetric hydrogen density

Bing Li[a,b], Yang Ding[b,c], Duck Young Kim[d,e], Rajeev Ahuja[f,g], Guangtian Zou[a,1], and Ho-Kwang Mao[a,b,e,1]

[a]State Key Laboratory of Superhard Materials, Jilin University, Changchun 130012, China; [b]High Pressure Synergetic Consortium, Carnegie Institution of Washington, 9700 South Cass Avenue, Argonne, IL 60439; [c]Advanced Photon Source, Argonne National Laboratory, Argonne, IL 60439; [d]Theory of Condensed Matter Group, Cavendish Laboratory, University of Cambridge, J. J. Thomson Avenue, Cambridge CB3 0HE, United Kingdom; [e]Geophysical Laboratory, Carnegie Institution of Washington, Washington, DC 20015; [f]Condensed Matter Theory Group, Department of Physics and Astronomy, Uppsala University, Box 530, SE-751 21 Uppsala, Sweden; and [g]Applied Material Physics, Department of Materials Science and Engineering, Royal Institute of Technology (Kungliga Tekniska Högskolan), SE-100 44 Stockholm, Sweden

Materials with very high hydrogen density have attracted considerable interest due to a range of motivations, including the search for chemically precompressed metallic hydrogen and hydrogen storage applications. Using high-pressure synchrotron X-ray diffraction technique and theoretical calculations, we have discovered a new rhodium dihydride (RhH$_2$) with high volumetric hydrogen density (163.7 g/L). Compressing rhodium in fluid hydrogen at ambient temperature, the fcc rhodium metal absorbs hydrogen and expands unit-cell volume by two discrete steps to form NaCl-typed fcc rhodium monohydride at 4 GPa and fluorite-typed fcc RhH$_2$ at 8 GPa. RhH$_2$ is the first dihydride discovered in the platinum group metals under high pressure. Our low-temperature experiments show that RhH$_2$ is recoverable after releasing pressure cryogenically to 1 bar and is capable of retaining hydrogen up to 150 K for minutes and 77 K for an indefinite length of time.

metal hydrides | phase transition

As the first and lightest element, hydrogen illustrates the richness of high-pressure physics. Wigner and Huntington (1) started with a simple conjecture that, above 25 GPa, hydrogen molecules would dissociate in favor of a monatomic metal. Hydrogen may also metalize in the molecular form by pressure-induced band-gap closure (2). Moreover, metallic hydrogen has been predicted to be a high-Tc superconductor (3, 4). However, direct compression of hydrogen up to the maximum achievable static pressure of 320 GPa was still insufficient to reach the predicted metallization pressure (5) which has been revised to >400 GPa by modern theories (4). Compression of hydrogen-rich metallic alloys has been suggested as an alternative way to attain the metallic hydrogen state (6). One may think of hydrogen atoms as being "chemically precompressed" in hydrides with a small H atomic volume, thus requiring less additional compression to a metallic high-Tc state than that for pure hydrogen. This suggestion has motivated a great deal of high-pressure theoretical and experimental research on hydrogen-rich alloys. Selected examples on MH$_4$ (where M = Si, Ge, Sn, or Pb) alone are shown in refs. 7–16.

Hydrogen has also been considered as an abundant and environmental-friendly fuel of the future, but onboard hydrogen storage remains a critical issue that hinders the application (17, 18). The ideal hydrogen storage material ought to satisfy a number of criteria, including high volumetric H density, high gravimetric H content, near ambient pressure–temperature condition for H absorption/discharge, and cost effectiveness (17, 18). Although no material has yet met all criteria, extreme limits of these criteria have been pursued and explored individually. Materials with extremely high H atomic ratio (n) have been synthesized in Xe(H$_2$)$_8$(n = 16) by high-pressure experiment (19), and NaH$_9$ (n = 9) by theory (20). BaReH$_9$ with a very high volumetric H density (134 g/L) has been predicted by theory (21) to chemically precompress its discrete H$_2$ units in the structure and cause a dramatic lowering of the metallization pressure to 51 GPa.

Hydrogen in metal hydrides (22) often exists in the atomic form, filling the octahedral (o) or tetrahedral (t) sites of the close-packed metal atoms (Fig. 1A). Hydrides of platinum group metals (PGM: Ru, Rh, Ir, Os, Pd, and Pt) are particularly interesting because of a number of favorable characteristics. For instance, the palladium hydride shows exceptional catalytic properties and kinetic reversibility (18) of hydrogen (23, 24). The shortcomings of the PGM hydrides, however, are their low gravimetric and volumetric H densities due to their high atomic mass and low n in MH$_n$ (all known PGM hydrides have n ≤ 1). Here we explored the possibility of increasing n significantly by pressure.

Rhodium with the fcc crystal structure (Fig. 1A, Bottom) has one o site and two t sites for each Rh atom. In the known rhodium monohydride (RhH) (25), hydrogen atoms fill the o site (Fig. 1A, Middle). We conducted ab initio zero-temperature calculations on enthalpies, phonon stabilities, and unit-cell volumes for various combinations of H filled o and t sites of Rh, and found an RhH$_2$ phase with H in two t sites (Fig. 1A, Top) standing out as the most stable hydride. It has a lower enthalpy and is thermodynamically more stable than RhH and Rh in a hydrogen-saturated high-pressure environment (Fig. 1B). Calculations of phonon dispersion curves and density of states (Fig. 1C) of RhH and RhH$_2$ also indicate that RhH$_2$ is dynamically stable to at least 90 GPa.

We conducted high-pressure experiments on Rh-H$_2$ up to 19 GPa, and indeed observed the formation of RhH$_2$ above 8 GPa. Rhodium powders were loaded in fluid H$_2$ in the sample chamber of an Re gasket and compressed with a diamond-anvil cell (DAC). A small ruby chip was placed in the sample chamber for pressure calibration. The crystal structure and volume of the Rh sample was probed with monochromatic angular dispersive high-pressure synchrotron X-ray diffraction (XRD) technique using synchrotron X-radiation. At room temperature up to 4.0 GPa, the observed XRD pattern corresponded to the pure rhodium sample with fcc structure (Fig. 2, Bottom). Compressing to 4.5 GPa, the RhH formed as a result of hydrogen absorption. The crystal symmetry and diffraction pattern remain fcc, but its unit-cell volume expands 15.5% (ΔV_1 = 9.9 Å^3) due to the filling of all o sites by H atoms (Fig. 2, Middle). This observation is consistent with the known NaCl-structured RhH (26). Further compressing to 8 GPa, we discovered the RhH$_2$ phase which remained in the fcc structure with another step of 21.2% unit-cell volume expansion (ΔV_2 = 15.4 Å^3). The abrupt volume expansion of the fcc unit cell clearly indicates the doubling of n and is consistent with the fluorite-structured RhH$_2$ with the H filling all t sites (Fig. 2, Top). Decompressing at room temperature, the
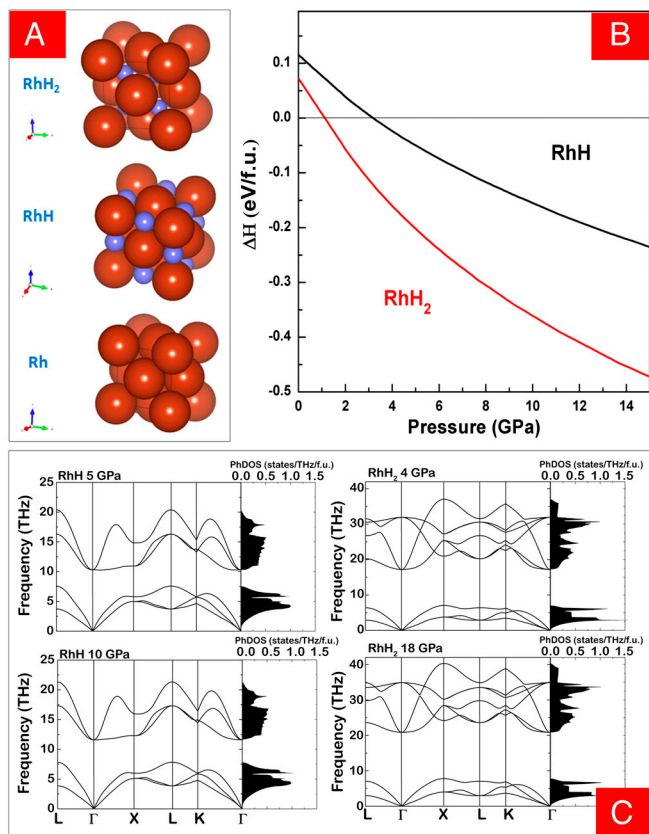
Fig. 1. Calculated and phonon dispersion of RhH and RhH$_2$ at zero temperature. (*A*) The Rh atoms (red) occupy fcc lattice points at (0, 0, 0); the H atoms (blue) occupy the octahedral sites at (½, ½, ½) in the RhH phase, and the tetrahedral sites at (¼, ¼, ¼) in the RhH$_2$ phase. (*B*) Enthalpy of formation. The reference state is the elements at the corresponding pressure—i.e., $\Delta H = H(\mathrm{RhH}_n) - H(\mathrm{Rh}) - nH(0.5\mathrm{H}_2)$ for each pressure. (*C*) Phonon dispersion curves and density of states (PhDOS) per formula unit (f.u.) in RhH at 5 and 10 GPa and RhH$_2$ at 4 and 18 GPa.

RhH$_2$ released H, transformed back to RhH, and finally to rhodium at 4 and 3 GPa, respectively.
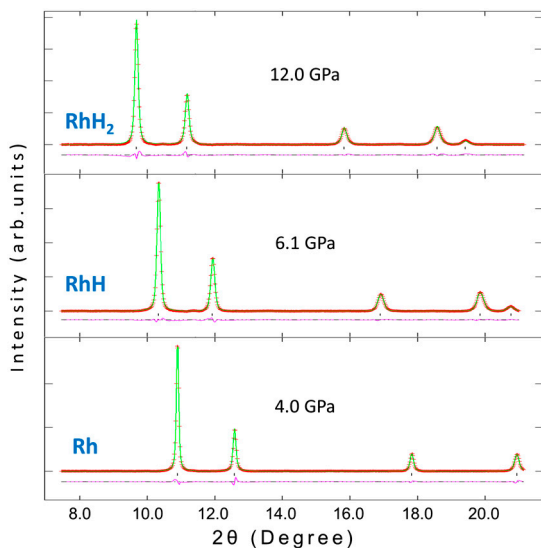

Fig. 2. In situ XRD patterns and crystal structures of Rh, RhH, and RhH$_2$. Experimental data, red crosses; full-profile refinements, green curves; difference patterns, pink curves (using General Structure Analysis System program); tick marks, peak positions calculated from the refined lattice parameters; X-ray wavelength, 0.41542 Å.

The large pressures hysteresis of hydrogen absorption–desorption at room temperature suggests the possibility of recovery of the new phase to ambient pressure if the reversal reaction can be retarded at low temperatures. We compressed the sample to 19 GPa at 300 K. After XRD confirmation of the complete conversion to RhH$_2$, we cooled the sample isobarically down to 6.1 K and decompressed isothermally at 6.1 K. The XRD patterns (Fig. 3*A*) obtained in situ during decompression clearly indicated that the high-pressure RhH$_2$ phase was quenchable to ambient pressure at low temperature. After the successful quenching of RhH$_2$ to ambient pressure, we continued the experiment by warming up the sample. Fig. 3*B* shows the evolution of XRD patterns of RhH$_2$ with rising temperature at the rate of approximately 25 K/h at ambient pressure. The RhH$_2$ was preserved up to the liquid nitrogen temperature (77 K). New XRD peaks corresponding to RhH appeared at 101 K. The intensities of RhH peaks grew at the expense of reducing RhH$_2$ peaks with rising temperature to 150 K, showing the releasing of hydrogen from RhH$_2$ and the conversion to RhH. Further warming up (Fig. 3*B*) depleted RhH$_2$, released hydrogen from RhH, and finally at 273 K, only Rh was present. We repeated the experiment to keep the RhH$_2$ at 78 K for a long time. After 10 h, 10% of the RhH$_2$ decomposed to RhH.

The pressure–volume (*P*–*V*) relation of Rh, RhH, and RhH$_2$ measured by the XRD are in excellent agreement with the theoretical calculations (Fig. 4*A*), thus confirming the stoichiometry of RhH and RhH$_2$. Unlike PdH$_n$ and many other metal hydrides whose volumes and *n* change continuously, the volume of RhH$_n$ changes sharply and discretely and indicates integer *n*. The RhH$_2$ XRD data at 6.1 K (Fig. 4*B*) can be fitted to a second-order Birch–Murnaghan *P*–*V* equation of state (assuming $K_0' = 4$):

$$P = (3/2)K_0[(V_0/V)^{7/3} - (V_0/V)^{5/3}],$$

where $K_0 = 194(3)$ GPa and $V_0 = 81.7(2)$ Å^3.

Although the NaCl-structured MH^o and fluorite-structured MH$^t_2$ are quite common among metal hydrides (22), their high-pressure transitions often involve other close phase structures such as hcp or deviation from stoichiometry (noninteger *n*). Rh actually stands out as the unique example of the elegant two-step hydrogen absorption–desorption, from metal (M) to MH^o and MH$^t_2$ by stepwise filling of *o* and *t* sites while keeping the fcc lattice unchanged. Similar to the intriguing pressure-induced volume expansion of zeolite (27), XRD only sees the Rh fcc lattice without seeing the addition of H, resulting in the apparent pressure-induced volume expansion of the Rh-RhH-RhH$_2$ series. Whereas all previously known PGM hydrides have $n \leq 1$ (22, 25), this RhH$_2$ stands out as one with $n = 2$, and the RhH$_2$ discovered at high pressure is recoverable at ambient pressure at liquid nitrogen temperature. With the tight bonding (thus small volume) of PGM and the larger *n*, RhH$_2$ at ambient pressure shows a very high volumetric H density of 163.7 g/L, which is one of the highest among all known hydrides and is 2.3 times higher than that of the liquid hydrogen. Finally, the present study demonstrates the power of combination and interaction of theory and experiment in design and synthesis interesting materials.

Methods

The electronic calculations presented here are based on the generalized gradient approximation with Perdew–Burke–Ernzerhof parameterization (28) for the exchange-correlation functional to density functional theory (29) using Vienna Ab-initio Simulation Package software (30). The ab initio lattice dynamics were performed with density functional perturbation theory using Quantum espresso software. The electronic wave function was expanded with a kinetic energy cutoff of 60 Ryd. Electronic calculations were converged with a $24 \times 24 \times 24$ Monkhorst–Pack (MP) (31) *k* mesh for Brillouin zone integration and a $12 \times 12 \times 12$ mesh was used for the phonon calculations. For calculations of solid hydrogen, an hcp phase (32) with 16 atoms in the unit cell was used with $8 \times 8 \times 8$ MP *k* mesh and 1,000 eV kinetic energy cutoff.

Fig. 3. In situ XRD patterns corresponding to the recovery of RhH$_2$ to ambient pressure at low temperature and its decomposition with temperature increased at 1 atm. (*A*) Decompression at 6.1 K; (*B*) warming up at ambient pressure; X-ray wavelength, 0.39804 Å. The diffraction peaks at 11°–12° marked with asterisks are from the gasket.

Fig. 4. Pressure dependence of unit-cell volumes of (*A*) Rh, RhH, and RhH$_2$ at 300 K and (*B*) RhH$_2$ at 6.1 K. Solid circles, experimental data points of Rh, RhH, and RhH$_2$ (red, compression; black, decompression); dashed curves, Birch-Murnaghan fit of the *P–V* data; dashed-dot curves, from theoretical calculation. The uncertainties in pressure are ±0.4 GPa, and the uncertainties in volume are smaller than the symbols.

Two sets of high-pressure experiments were conducted on the Rh-H$_2$ system: one at room temperature up to 16.5 GPa and decompressing to 1 atm, and the other up to 19 GPa, cooling down to 6.1 K, decompressing to 1 atm, and warming to room temperature. In situ XRD patterns were measured along the pressure–temperature pathways at 16ID-B station of the High-Pressure Collaborative Access Team Sector, Advanced Photon Source, Argonne National Laboratory. The Rh powder sample (99.99% purity) was compacted into a foil and placed in the gasket hole of a DAC. Hydrogen gas was introduced into the sample chamber at 0.17 GPa and acted as both a chemical reactant and a physical pressure-transmitting medium. A clear transparent area around rhodium or rhodium hydride was optically visible at all pressures, indicating the presence of free hydrogen in the sample chamber. Pressures were measured using the ruby fluorescence technique. The room temperature experiment was conducted with diamond anvils of 300-μm diameter, Re gasket with 250-μm initial thickness preindented to 65-μm thickness with a hole (sample chamber) of 100 μm, and X-ray wavelength of 0.41542 Å, focused down to 10 × 10 μm at the sample position. The low-temperature experiment was conducted in a liquid-flow He cryostat, with diamond anvils of 500-μm diameter, stainless steel gasket with 250-μm initial thickness preindented to 25-μm thickness with a hole of 200 μm, and X-ray wavelength of 0.39804 Å, focused through cryostat windows down to 50 × 50 μm onto the sample. A motor-controlled gear box was used to adjust pressure during the low-temperature experiment. The XRD patterns were integrated using the Fit2D software and analyzed using General Structure Analysis System.

1. Wigner E, Huntington HB (1935) On the possibility of a metallic modification of hydrogen. *J Chem Phys* 3:764–770.
2. Mao HK, Hemley RJ (1994) Ultrahigh-pressure transitions in solid hydrogen. *Rev Mod Phys* 66:671–692.
3. Ashcroft NW (1968) Metallic hydrogen: A high-temperature superconductor? *Phys Rev Lett* 21:1748–1750.
4. Barbee TWI, Garcia A, Cohen ML (1989) First-principles prediction of high-temperature superconductivity in metallic hydrogen. *Nature* 340:369–371.
5. Loubeyre P, Ocelli F, LeToullec R (2002) Optical studies of hydrogen to 320 GPa and evidence for black hydrogen. *Nature* 416:613–617.
6. Ashcroft NW (2004) Hydrogen dominant metallic alloys: High temperature superconductors? *Phys Rev Lett* 92:187002.
7. Feng J, et al. (2006) Structures and potential superconductivity in SiH_4 at high pressure: En route to "metallic hydrogen". *Phys Rev Lett* 96:017006.
8. Pickard CJ, Needs RJ (2006) High-pressure phases of silane. *Phys Rev Lett* 97:045504.
9. Eremets MI, Trojan IA, Medvedev SA, Tse JS, Yao Y (2008) Superconductivity in hydrogen dominant materials: Silane. *Science* 319:1506–1509.
10. Martinez-Canales M, et al. (2009) Novel structures and superconductivity of silane under pressure. *Phys Rev Lett* 102:087005.
11. Strobel TA, Somayazulu M, Hemley RJ (2009) Novel pressure-induced interactions in silane-hydrogen. *Phys Rev Lett* 103:065701.
12. Yim W-L, Tse JS, Iitaka T (2010) Pressure-induced intermolecular interactions in crystalline silane-hydrogen. *Phys Rev Lett* 105:215501.
13. Gao GY, et al. (2008) Superconducting high pressure phase of germane. *Phys Rev Lett* 101:107002.
14. Tse JS, Yao Y, Tanaka K (2007) Novel superconductivity in metallic SnH_4 under high pressure. *Phys Rev Lett* 98:117001–117004.
15. Zeleski-Ejgierd P, Ashcroft NW, Hoffmann R (2011) High pressure stabilization and emergent forms of PbH_4. *Phys Rev Lett* 107:037002.
16. Kim DY, Scheicher RH, Mao HK, Kang TW, Ahuja R (2010) General trend for pressurized superconducting hydrogen-dense materials. *Proc Natl Acad Sci USA* 107:2793–2796.
17. Schlapbach L, Züttel A (2001) Hydrogen-storage materials for mobile applications. *Nature* 414:353–358.
18. Grochala W, Edwards PP (2004) Thermal decomposition of the non-interstitial hydrides for the storage and production of hydrogen. *Chem Rev* 104:1283–1315.
19. Somayazulu M, et al. (2010) Pressure-induced bonding and compound formation in xenon–hydrogen solids. *Nat Chem* 2:50–53.
20. Baettig P, Zurek E (2011) Pressure-stabilized sodium polyhydrides: NaH_n ($n > 1$). *Phys Rev Lett* 106:237002.
21. Markopoulos G, Kroll P, Hoffmann R (2010) Compressing the most hydrogen-rich inorganic ion. *J Am Chem Soc* 132:748–755.
22. Fukai Y (2005) *The Metal-Hydrogen System: Basic Bulk Properties* (Springer, Berlin) p 497.
23. Mitsui T, Rose MK, Fomin E, Ogletree DF, Salmeron M (2003) Dissociative hydrogen adsorption on palladium requires aggregates of three or more vacancies. *Nature* 422:705–707.
24. Lopez N, Łodziana Z, Illas F, Salmeron M (2004) When Langmuir is too simple: H2 dissociation on Pd(111) at high coverage. *Phys Rev Lett* 93:146103.
25. Antonov VE, Belash IT, Malyshev VY, Ponyatovsky EG (1984) The solubility of hydrogen in the platinum metals under high pressure. *Platinum Met Rev* 28:158–163.
26. Somenkov VA, Glazkov VP, Irodova AV, Shilstein SS (1987) Crystal structure and volume effects in the hydrides of d metals. *J Less-Common Met* 129:171–180.
27. Lee Y, Vogt T, Hriljac JA, Parise JB, Artioli G (2002) Pressure-induced volume expansion of zeolites in the natrolite family. *J Am Chem Soc* 124:5466–5475.
28. Perdew JP, Burke K, Ernzerhof M (1996) Generalized gradient approximation made simple. *Phys Rev Lett* 77:3865–3868.
29. Kohn W, Sham LJ (1965) Self-consistent equations including exchange and correlation effects. *Phys Rev* 140:A1133–A1138.
30. Kresse G, Furthmüller J (1996) Efficiency of ab-initio total energy calculations for metals and semiconductors using a plane-wave basis set. *Comput Mater Sci* 6:15 50.
31. Monkhorst HJ, Pack JD (1976) Special points for Brillouin-zone integrations. *Phys Rev B Condens Matter Mater Phys* 13:5188–5192.
32. Pickard CJ, Needs RJ (2007) Structure of phase III of solid hydrogen. *Nat Phys* 3:473–476.

PHYSICS